Earth and Planetary Science Letters 417 (2015) 67–77

Contents lists available at ScienceDirect

Earth and Planetary Science Letters

www.elsevier.com/locate/epsl

# Deformation of a crystalline olivine aggregate containing two immiscible liquids: Implications for early core–mantle differentiation

V. Cerantola [a], N.P. Walte [a,b,*], D.C. Rubie [a]

[a] Bayerisches Geoinstitut, Universität Bayreuth, D-95440 Bayreuth, Germany
[b] Forschungs-Neutronenquelle Heinz Maier-Leibnitz, Technische Universität München, Garching, Germany

ARTICLE INFO

*Article history:*
Received 27 October 2014
Received in revised form 9 February 2015
Accepted 11 February 2015
Available online 5 March 2015
Editor: J. Brodholt

*Keywords:*
core–mantle differentiation
melt segregation
deformation experiments
olivine
multianvil

ABSTRACT

Deformation-assisted segregation of metallic and sulphidic liquid from a solid peridotitic matrix is a process that may contribute to the early differentiation of small planetesimals into a metallic core and a silicate mantle. Here we present results of an experimental study using a simplified system consisting of a polycrystalline $Fo_{90}$-olivine matrix containing a small percentage of iron sulphide and a synthetic primitive MORB melt, in order to investigate whether the silicate melt enhances the interconnection and segregation of FeS liquid under deformation conditions at varying strain rates. The experiments have been performed at 2 GPa, 1450 °C and strain rates between $1 \times 10^{-3}$ $s^{-1}$ to $1 \times 10^{-5}$ $s^{-1}$. Our results show that the presence of silicate melt actually hinders the migration and segregation of sulphide liquid by reducing its interconnectivity. At low to moderate strain rates the sulphide liquid pockets preserved a roundish shape, showing the liquid behavior is governed mainly by surface tension rather than by differential stress. Even at the highest strain rates, insignificant FeS segregation and interconnection were observed. On the other hand the basaltic melt was very mobile during deformation, accommodating part of the strain, which led to its segregation from the matrix at high bulk strains leaving the sulphide liquid stranded in the olivine matrix. Hence, we conclude that deformation-induced percolation of sulphide liquid does not contribute to the formation of planetary cores after the silicate solidus is overstepped. A possible early deformation enhanced core–mantle differentiation after overstepping the Fe–S solidus is not possible between the initial formation of silicate melt and the formation of a widespread magma ocean.



## 1. Introduction

The differentiation of planetary bodies with radii larger than ~30 km into a metallic core and a silicate mantle was one of the earliest and most important events in the history of the Solar System (Rubie et al., 2007; Wood et al., 2006; Stevenson, 1990). After the first stages of accretion, the undifferentiated material underwent a rapid (<1 Ma, Kruijer et al., 2014) reorganization that separated dense Fe–Ni–S liquid from the less-dense silicate materials. The main heat source for the differentiation of smaller bodies is the decay of the short-lived radioactive isotopes $^{26}Al$ and $^{60}Fe$, which according to simulations caused complete melting if the planetesimals accreted to a certain size (radius of 20–80 km) shortly after Solar System formation (<2 Ma) (Hevey and Sanders, 2006; Gupta and Sahijpal, 2010). During such a magma ocean stage the denser metallic and sulphidic liquid droplets could sink rapidly through the silicate melt to form a core, a process which is generally agreed to have occurred during the final differentiation of terrestrial planets (e.g. Stevenson, 1990; Rubie et al., 2003, 2007). However, in the case of planetesimals, studies that have included the transport of the lithophile $^{26}Al$ towards the surface with the first silicate melts, questioned whether a complete melting stage could be reached and suggested a differentiation of a core and a basaltic crust from an only partially molten mantle (Wilson and Keil, 2012; Neumann et al., 2014). This consideration and the rapid core-formation inferred from dating iron meteorites (Kruijer et al., 2014) suggest that differentiation processes that do not rely on complete melting may be important including (i) liquid migration and differentiation after crossing the sulphide solidus, and (ii) differentiation after crossing the silicate solidus (the Fe–S solidus is overstepped before the silicate solidus e.g. Walter and Trønnes, 2004). Here, we show that although these two regimes are only separated by a small temperature interval, they are completely different with regard to core–mantle differentiation processes.

* Corresponding author at: Bayerisches Geoinstitut, Universität Bayreuth, D-95440 Bayreuth, Germany.
*E-mail address:* nico.walte@uni-bayreuth.de (N.P. Walte).

http://dx.doi.org/10.1016/j.epsl.2015.02.014

### 1.1. Differentiation after crossing the sulphide solidus

Grain-scale percolation of an interconnected Fe–S liquid through a solid silicate matrix has long been suggested to be an important mechanism of planetary differentiation (Bruhn et al., 2000; Yoshino et al., 2003; Hustoft and Kohlstedt, 2006; Terasaki et al., 2008). This differentiation mechanism has recently gained credibility due to the study of Kruijer et al. (2014) that showed that the time of differentiation of iron meteorites correlates with the sulphur content in the iron. This observation is best explained by the lower melting point and the lower dihedral angle of Fe–S when in contact with olivine that aids liquid interconnection in a solid matrix. At low pressure and under oxidizing conditions such liquids might even form a fully interconnected network (Terasaki et al., 2008).

If and to which degree molten metal can segregate from a solid silicate matrix, depends on the ability of the liquid phase to form an interconnected network. In a hydrostatic system this is mainly determined by the liquid fraction and the dihedral angle $\theta$ formed at a triple junction between a liquid pocket and two grains (e.g. Bulau et al., 1979). A threshold angle of 60° divides a regime in which a low-percentage liquid phase is distributed as a fully interconnected network within the matrix ($\theta < 60°$) from one in which it is trapped as isolated liquid pockets ($\theta > 60°$) (Bulau et al., 1979; Von Bargen and Waff, 1986). Fe-alloy and FeS liquids usually have a dihedral angle higher than 60° in an olivine matrix (e.g. Ballhaus and Ellis, 1996; Rose and Brenan, 2001; Terasaki et al., 2005; 2008). In simulations such liquids require a $\theta$-dependent critical melt fraction between 2 vol.% and 6 vol.% to allow interconnection (Von Bargen and Waff, 1986). Experimental studies of *in situ* electrical conductivity measurements showed that for FeS liquid in an olivine matrix the connectivity threshold is approximately 5 vol.%, which means that partial core–mantle differentiation may be possible (Yoshino et al., 2003, 2004). However, other authors argued that a higher percentage should be present in the matrix to allow a fully interconnected liquid network (Bagdassarov et al., 2009a; Walte et al., 2007). Regardless of the exact threshold, it is clear that some residual liquid must remain trapped in the matrix so that static percolation alone cannot produce efficient core–mantle differentiation as required on geochemical grounds (e.g. Wood et al., 2006).

Deformation-induced interconnection in olivine/peridotite-metallic liquid aggregates has been investigated in several experimental studies as a candidate for lowering this percentage of stranded liquid (Bruhn et al., 2000; Hustoft and Kohlstedt, 2006; Groebner and Kohlstedt, 2006; Rushmer et al., 2005; Walte et al., 2011). All studies have agreed that deformation has the potential to mobilize Fe–S liquids and lower the percentage of stranded liquid with estimations ranging from $\ll 1$ vol.% (Groebner and Kohlstedt, 2006) to 2–3 vol.% (Walte et al., 2011) as long as the differential stress or strain rate is sufficient to overcome the capillary forces of the liquid (Groebner and Kohlstedt, 2006; Walte et al., 2011).

### 1.2. Differentiation after overstepping the silicate solidus

Few experimental studies have been performed that consider the effect of silicate melt formation. Fe–Ni–S liquids and silicate melts are immiscible, i.e. the interplay of two melts with different dihedral angles and a crystalline matrix have to be considered to evaluate the potential for differentiation. Experiments on partially molten chondritic material (Rushmer et al., 2005; Rushmer and Petford, 2011), and experiments under static conditions (Holzheid, 2013) indicated that the presence of silicate melt does not enhance segregation, while a centrifuge study of Fe–S liquid settling indicated an enhancement of Fe–S migration at a moderate fraction of silicate melt compared to the melt-free case (Bagdassarov et al., 2009b). Here, we present the results of controlled deformation experiments performed to systematically investigate the effect of a small fraction of an immiscible silicate melt phase on the microstructure and distribution of liquid FeS in an olivine matrix. This simplified system simulates a planetary body in which the temperature just oversteps the silicate solidus.

## 2. Methods

Deformation experiments were performed with the MAVO six-ram press, a multianvil device with six independently controlled anvils that enables deformation and static experiments to be performed at upper mantle and transition zone pressure and temperature conditions (Manthilake et al., 2012). The experiments were performed by pure shear, i.e. one compression axis, one retracting axis, and one neutral axis. The deformed samples were sectioned in the $x$–$z$ orientation, i.e. the plane containing the longest and shortest axes of the strain ellipsoid. Two static experiments, one with the MAVO press and one with a conventional deformation-DIA press (Wang et al., 2003) were performed for comparison. In addition to enabling pure shear deformation, the strain rate control of the MAVO press is more precise than of the d-DIA.

Experiments have been carried out using cubic 8/6 assemblies (cube edge length / anvil truncation size in millimeters) with the cubic pressure medium and external gaskets consisting of unfired pyrophyllite. Temperature was monitored by a D-type thermocouple that was in contact with the top of the sample capsule. The assemblies contained a stepped graphite furnace to reduce the thermal gradient (e.g. Manthilake et al., 2012). The systematic error due to the location of the thermocouple junction is estimated to be within 50 K; however, since all experiments were performed with identical assembly and sample capsule designs, the statistical error between experiments is likely lower. Samples consisted of synthetic olivine powder with a chemical composition of $(Mg_{0.90}Fe_{0.10})_2SiO_4$ that was mechanically mixed with 5 wt.% iron sulphide and 9 wt.% of a synthetic calc-alkaline primitive mid-ocean ridge basalt (MORB), which at the experimental conditions does not react with the olivine matrix. The silicate melt (BM) was calculated to be in equilibrium with an empirical depleted mantle composition (Kinzler and Grove, 1992) and was renormalized to exclude $K_2O$ and $TiO_2$. The amount of silicate liquid was observed to be sufficient to ensure clearly visible microstructures between the three phases. The experimental run M175 was executed without the presence of basaltic melt; however, the FeS content was kept at 5 wt.%. The decision to keep 5 wt.% of FeS in all experiments was twofold: (i) to obtain results compatible with those of a previous experimental study on olivine–FeS liquid deformation (Walte et al., 2011); (ii) this value is below the critical connectivity threshold for static systems of 5 vol.% according to Yoshino et al. (2003); hence, any connection and segregation of FeS liquid observed in the experiments can be assumed to be due to deformation.

The starting mixture was loaded in Re capsules with a height of 1.5 mm and a diameter of 1.6 mm. Experiments were performed at 2 GPa and 1450 °C, which is above the FeS and basaltic melt liquidus (Walter and Trønnes, 2004). Under these experimental conditions the FeS dihedral angle is ≈75° (Walte et al., 2007), whereas for the silicate melt the dihedral angle is significantly below 60°. After cold compression and heating, the samples were annealed at 1450 °C for one to two hours in order to achieve local equilibrium before deformation commenced (Fig. 1). Earlier experiments revealed that this annealing time was sufficient to achieve textural equilibrium of the liquid FeS pockets and that the liquid-pocket shape did not change significantly after longer annealing times. The strain and strain rate were controlled externally by the

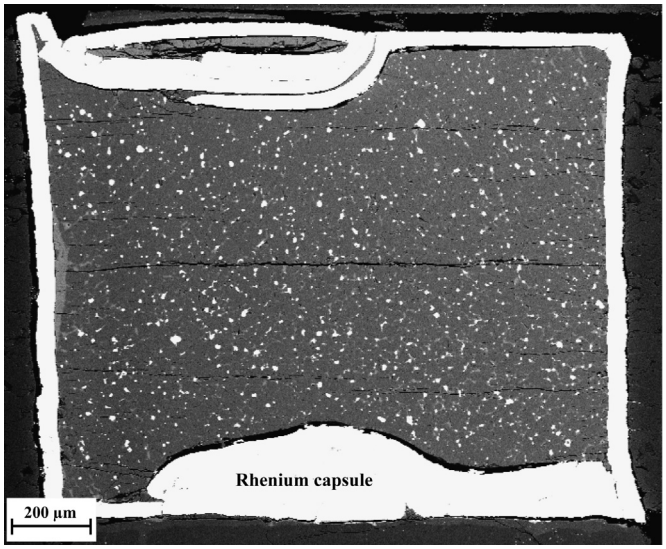


**Fig. 1.** Overview of an MAVO sample after 2 h static annealing at 2 GPa and 1450 °C (M176). The sample is composed of the olivine matrix (dark grey), basaltic melt (light grey), and FeS liquid pockets (white dots).

advancement and advancement rate of the deformation anvils. This leads to some uncertainty of sample strain rate since some of the strain may be accommodated by the assembly parts, which means that the values given in Table 1 represent an upper limit. However, the error is small for axial compression or pure shear deformation (less than 10%, based on measured length changes of the recovered samples compared to the bulk shortening). Furthermore, such a systematic error would be similar in all experiments since the assemblies were always identical.

Samples were bulk shortened by 4%, 15%, or 35% of the initial capsule length, henceforth referred as low, moderate, and high finite strain experiments, respectively. The strain rate of the experiments varied from $1 \times 10^{-3}$ to $1 \times 10^{-5}$ $s^{-1}$ (Table 1), but was held constant during individual experiments. All results of deformation experiments reported here were obtained with the MAVO press due to the superior strain rate control compared to the d-DIA. Liquid FeS alloys with the Re sample capsule and basaltic melt were found to be partially extruded from the sample capsule. Hence, the system was partially open with respect to melt expulsion. After a rapid quench within seconds (by switching off the power supply) and decompression, the recovered samples were embedded in epoxy, ground and polished, and subsequently analyzed with an LEO Gemini 1530 scanning electron microscope (SEM) at 20 or 30 kV voltage and 4 nA beam current. Sample imaging was performed by SEM secondary electron (SE), back-scattered electron (BSE) and orientation contrast analysis (OC). Image analyses were performed using the freeware ImageJ, a Java-based image processing program developed by the US National Institutes of Health. The greyscale SEM-BSE images were transformed into binary images highlighting the FeS liquid pockets and analyzed statistically. In this way the average sulphide liquid fraction, and the distribution and size of liquid pockets were determined in the quenched samples after deformation as described in Walte et al. (2011). Due to the often irregular shape of liquid pockets, the liquid pocket area is expressed in radii of equivalent circles, and the 2-D results are plotted in bar diagrams with a bin-size of 1 µm, which allows the sulphide liquid distribution of different experiments to be compared e.g. as a function of strain rate or the presence of the silicate liquid as described in Walte et al. (2011). While the 2-D size distributions presented in this study do not represent the true 3-D distribution due to the sectioning effect, the observed changes in 2-D distribution are expected to reflect true changes in the 3-D liquid pocket distribution.

## 3. Results

### 3.1. Static experiments

Two static experiments were performed in order to make a comparison with the microstructures generated by deformation. The sulphide liquid fraction after the static experimental runs is 3.9 vol.% for both samples (Table 1); hence, ~4 vol.% was taken as a base-line for the liquid fraction before deformation. The samples are characterized by a regular distribution of both immiscible liquid phases that are clearly distinguishable in the SEM images (Figs. 1–2). Higher magnification shows that the basalt forms an interconnected network, with melt-filled convex-inwards triple junctions that are typical for liquids with dihedral angles below 60° (Fig. 2b) (e.g. Von Bargen and Waff, 1986). The FeS liquid forms isolated and roundish droplets that are largely hosted by the silicate melt network (Fig. 2). In some places where FeS droplets are directly in contact with surrounding olivine grains, they exhibit elongation or an irregular shape (Fig. 2b), which may be a result of ongoing static recrystallization (Walte et al., 2003). In a few cases, the FeS is present as spherical liquid inclusions contained within larger olivine crystals (Fig. 2a), which indicates local abnormal grain growth of olivine (Walte et al., 2007).

Fig. 2 shows the sulphide liquid distribution over the bulk of the sample after three hours of static annealing. The binary image highlights the generally spherical shape of FeS liquid pockets (black) that is an indication of surface energy minimization of the high dihedral angle liquid; the bar diagram shows the range of liquid-pocket sizes characteristic for static experiments with high-dihedral-angle liquids. More than 60 vol.% of the total sulphide is present as small to medium size liquid pools (<5 µm radius). The amount of liquid in pockets ≤1 µm radius is slightly less than the combined amount in medium-large liquid pockets with a radius ≥5 µm (Fig. 2). Although the general spherical shape of the liq-

**Table 1**
Summary of d-DIA and MAVO press experiments. All experiments were performed at 2 GPa and 1450 °C.

| No. | Liquid* | Strain rate ($s^{-1}$) | Shortening (%) ** | BM before quench (wt.%) | FeS after quench (vol.%) | $\sigma^{(1)}$ |
|---|---|---|---|---|---|---|
| DD564 | FeS-BM | Static | – | 9 | 3.9 | 0.3 |
| M176 | FeS-BM | Static | – | 9 | 3.9 | 0.4 |
| M160 | FeS-BM | $1 \times 10^{-3}$ | 15 | 9 | 3.9 | 0.3 |
| M157 | FeS-BM | $1 \times 10^{-4}$ | 15 | 9 | 4.1 | 0.3 |
| M172 | FeS-BM | $1 \times 10^{-5}$ | 15 | 9 | 4.3 | 0.9 |
| M175 | FeS | $1 \times 10^{-4}$ | 15 | – | 3.1 | 0.1 |
| M177 | FeS-BM | $1 \times 10^{-4}$ | 35 | 9 | 2.7 | 0.4 |

$\sigma^{(1)}$ Standard deviation of FeS (vol.%) after quench.
* Liquid phases present in the system during the experiment: iron sulfide (FeS) and basaltic melt (BM).
** The capsule's initial length: 1500 µm.

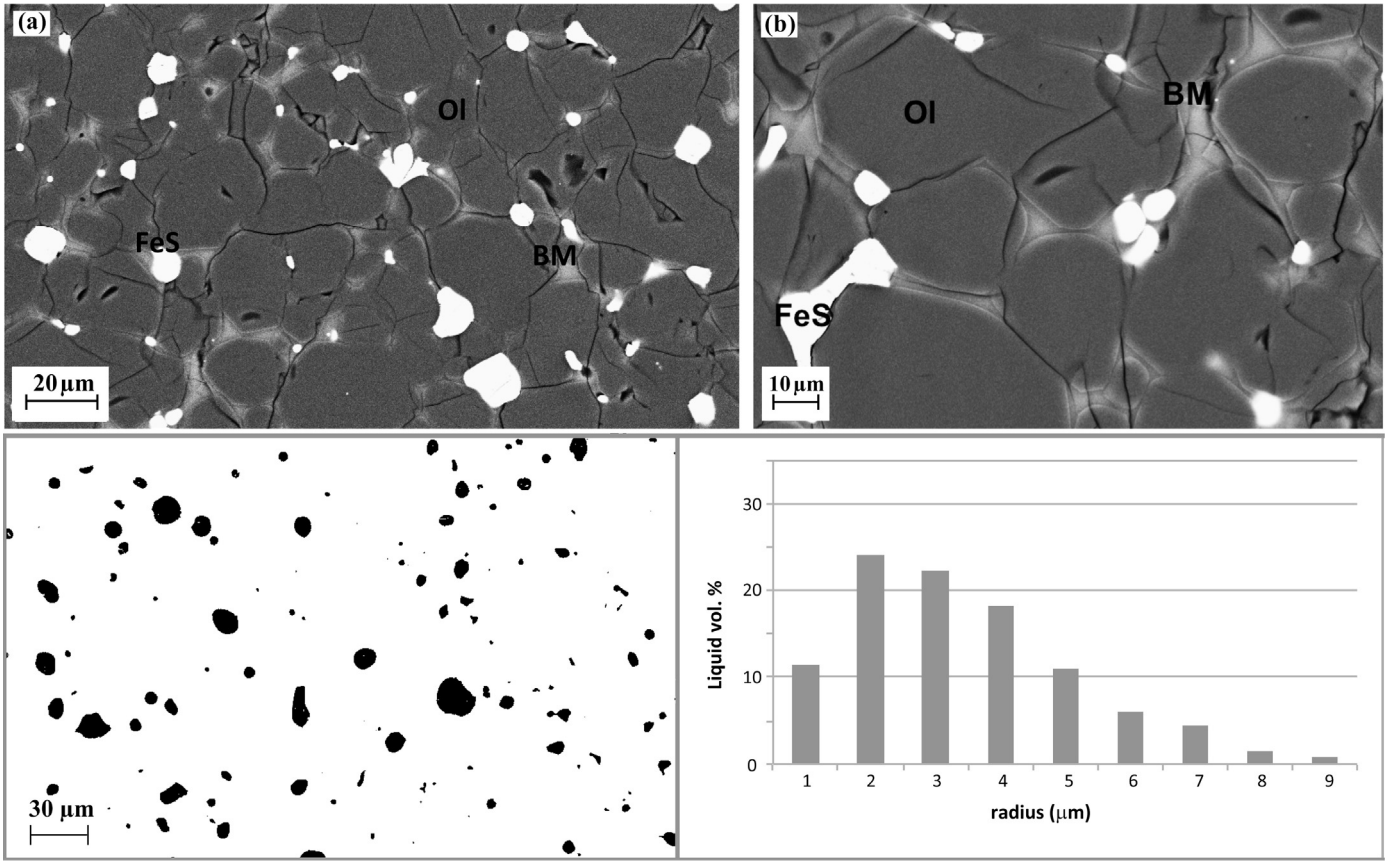


**Fig. 2.** Silicate melt and FeS liquid distribution in the static experiment M176. (a–b) Two SEM-BSE images of the quenched microstructure showing the iron sulphide liquid blobs (FeS) in white, basaltic melt (BM) in light grey, and olivine crystals in dark grey (Ol). The iron sulphide is situated within the silicate melt as roundish droplets. Note the sulphide pockets that are apparently in contact but have not yet coalesced. (Bottom) Liquid distributions in M176 showing the binary image of the FeS pockets and the liquid pocket size distribution depicted in a histogram that plots the liquid-fraction residing in liquid-pockets of a given size range (see Section 2 for details).

uid pockets and the smoothly curved grain boundaries indicate a locally equilibrated microstructure, the static sulphide liquid distribution does not represent a true textural equilibrium, as the lowest energy would be attained by complete removal of the sulphide liquid from the system (e.g. Jurewicz and Watson, 1985). The distribution rather reflects the particular starting mixture, a low liquid pocket mobility, and the annealing time.

### 3.2. Deformation experiments with low to moderate finite shortening

A first set of deformation experiments was performed at varying strain rates and a low finite shortening of 4% to investigate the microstructural evolution at the very beginning of deformation. However, the quenched microstructures were indistinguishable from those of the static microstructures described above, which indicates that the strain was not sufficient for liquid redistribution, perhaps because the first strain increment was buffered by the compaction of the other assembly parts. Hence, the subsequent experiments were shortened by 15% of their initial capsule length at systematically changing strain rates. In these experiments the amount of silicate and sulphide liquid in the quenched samples was similar to that of the static samples (Table 1), which indicates that there was little silicate or sulphide liquid separation taking place under these conditions.

#### 3.2.1. Microstructure

In the moderate finite strain experiments there is a clear correlation between the liquid microstructure and the applied strain rate (Fig. 3). The result of fast deformation is the formation of some elongated and distorted FeS liquid pockets and a slightly reduced amount of silicate melt. However, compared to previously published studies on systems free of silicate melt (Bruhn et al., 2000; Groebner and Kohlstedt, 2006; Walte et al., 2011), the elongation and distortion of the sulphide liquid is much reduced and is only clearly evident at the highest strain rates (Suppl. Fig. 1). At a high strain rate of $1 \times 10^{-3}$ $s^{-1}$ (Fig. 3a), large liquid FeS pockets are often stretched and deformed with an elongation sub-parallel to the shortening direction. Other less elongated FeS pools do not conserve the smooth spherical shape observed at lower strain rates, but rather display an irregular frayed shape in contact with olivine grains. Only smaller FeS pools preserve a roundish shape at the high deformation rate (Fig. 3a). On the other hand, at a low strain rate of $1 \times 10^{-5}$ $s^{-1}$, the liquid microstructure is indistinguishable from the static experiments, the FeS liquid pockets show a spherical shape and little elongation (Fig. 3c, Suppl. Fig. 1), and the silicate melt network appears little altered by deformation. At a medium strain rate, $1 \times 10^{-4}$ $s^{-1}$ (Fig. 3b), the system also appears to be dominated more by the phases' surface energy than by the applied differential stress. FeS liquid pockets largely retain an equant shape with only rare elongation; however, some liquid pockets show a frayed structure in contact with olivine grains. The silicate melt network appears to be slightly altered, showing a preferential orientation of wetted grain boundaries sub-parallel to the shortening direction as described previously, e.g. by Rosenberg and Handy (2001). To summarize, deformation causes only a small to moderate elongation of liquid pockets compared to silicate melt free experiments, and little evidence is found for a preferred orientation of the elongated liquid pockets at any strain rate (Suppl. Fig. 1).

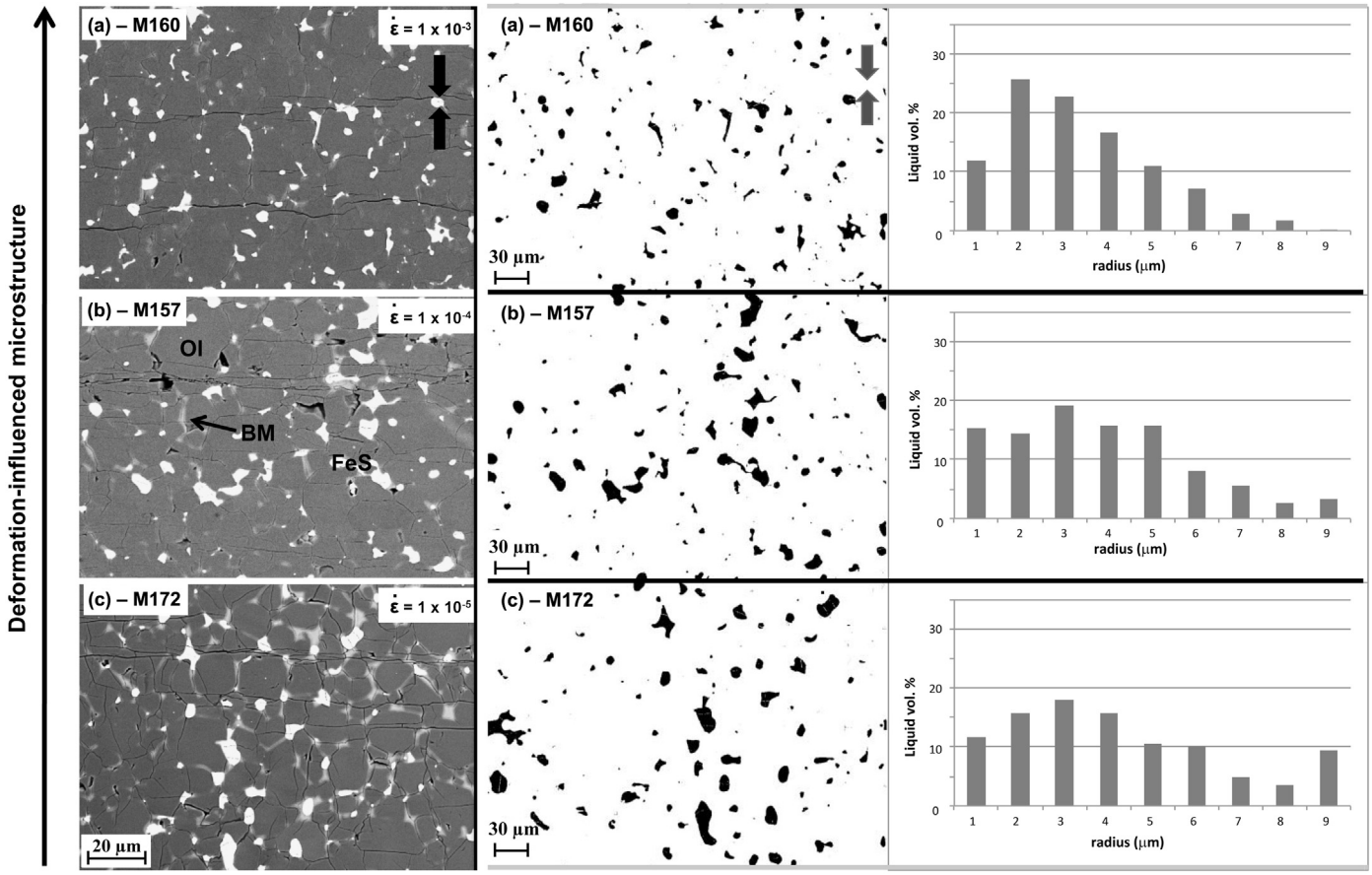


**Fig. 3.** Deformation microstructure and liquid distribution as a function of the strain rate (15% shortening). The FeS liquid is only clearly elongated by deformation at the highest strain rate ($1 \times 10^{-3}$ $s^{-1}$), while the microstructure of the lowest and intermediate strain rate is almost identical to static microstructures. Hence, the differential stress of the latter experiments was insufficient to elongate most liquid pockets (see also Suppl. Fig. 1). The histogram plots the liquid-fraction residing in liquid-pockets of a given size range; it shows that the higher the strain rate the more FeS resides in smaller liquid pockets.

### 3.2.2. Liquid distribution

Statistical analyses were performed in order to investigate the FeS liquid-pocket-size distribution as a function of strain rate (Fig. 3). The lower the strain rate, the larger the average liquid pocket size and the more liquid is located in large liquid pockets, as also observed in olivine–FeS liquid experiments (Walte et al., 2011). Interestingly, the average FeS liquid pocket size of samples deformed at moderate to low strain rates is generally larger than in the static experiments, which suggests liquid accumulation during deformation in contrast to the liquid dispersion observed in olivine–FeS experiments of Walte et al. (2011). Only at the highest strain rate is the sulphide pocket-size population similar to that of the static experiments (cf. Fig. 2 and Fig. 3), which indicates that liquid accumulation and liquid dispersion processes are balanced under these conditions.

### 3.3. Varying finite strain and sample composition

Two experiments were performed to investigate the effect of (a) higher finite strain (M177) and (b) a lack of silicate melt (M175) compared to the experiments described above. M175 contained a silicate-melt free starting powder composed of olivine and FeS, whereas the starting material of the sample M177 consisted of the standard three-phase mixture (Table 1). Both experiments were deformed at identical strain rates ($1 \times 10^{-4}$ $s^{-1}$) but with different finite strains. The silicate melt free sample (M175) was shortened by 15% ("moderate" finite strain), and the three-phase mixture (M177) was shortened by 35% ("high" finite strain). Despite their different starting composition, both samples showed a similar deformation microstructure that is characterized by the visible absence of basaltic melt after the quench (Fig. 4). Thus, in contrast to the moderate finite strain experiments described in Section 3.2, the higher finite strain induced a separation of the silicate melt, which was pushed out of the sample and capsule while leaving the sulphide liquid inside; thus the composition changed to that of a two-phase system. Accordingly, at the end stages of deformation both experiments experienced similar conditions, namely olivine–FeS liquid deformation at a strain rate of $1 \times 10^{-4}$ $s^{-1}$, which is reflected in almost identical microstructures and liquid distribution (Fig. 5). This similarity suggests that the preserved microstructures were mainly generated towards the end of the experiments and there is little memory of the early stages. The sulphide liquid pockets are generally elongated or highly irregular in shape, smaller liquid pockets are often aligned in linear FeS-rich zones that are characterized by a near vertical or inclined alignment (Fig. 4). These grain-scale shear zones locally wet the grain boundaries, thus allowing the occurrence of strain localization between the grains and the establishment of possible small-scale permeability and segregation (Walte et al., 2011). Elongation and pinch-off of larger liquid pools with diameters above ~2 µm results in a liquid-FeS distribution characterized by a high abundance of small sulphide droplets with radii <3 µm (Fig. 5) in both experiments. There is a rare occurrence of larger liquid pockets as observed in the silicate melt bearing experiments. In contrast to the experiments described above, in which the sulphide liquid fraction remains similar to that of static experiments (indicating no FeS liquid segregation), the iron sulphide liquid fraction of both experiments shows decreases to 3.1 vol.% and 2.7 vol.% after the

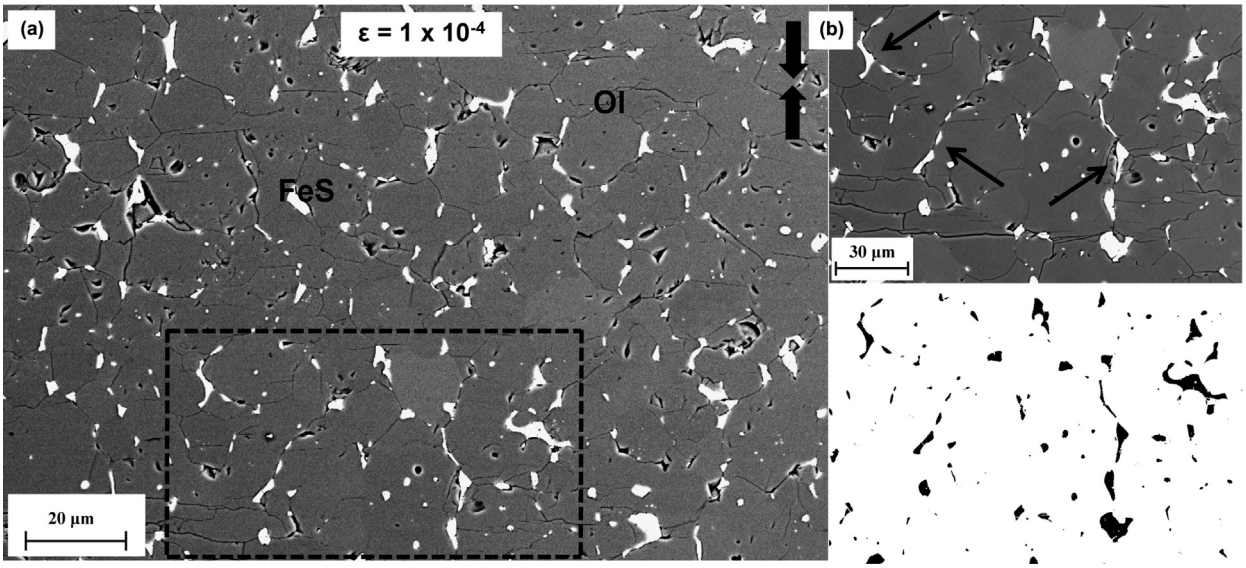


**Fig. 4.** BSE images of the silicate melt-free sample M175 (15% shortening). (a) Overview of the microstructure: FeS liquid pockets display elongated and highly distorted shapes. (b) BSE and binary image close-up of the region highlighted by the dashed square. Pinch-off of larger elongated liquid pockets produces chains of smaller liquid pockets, which is a mechanism for liquid dispersion. Black arrows in (a) indicate the shortening direction.

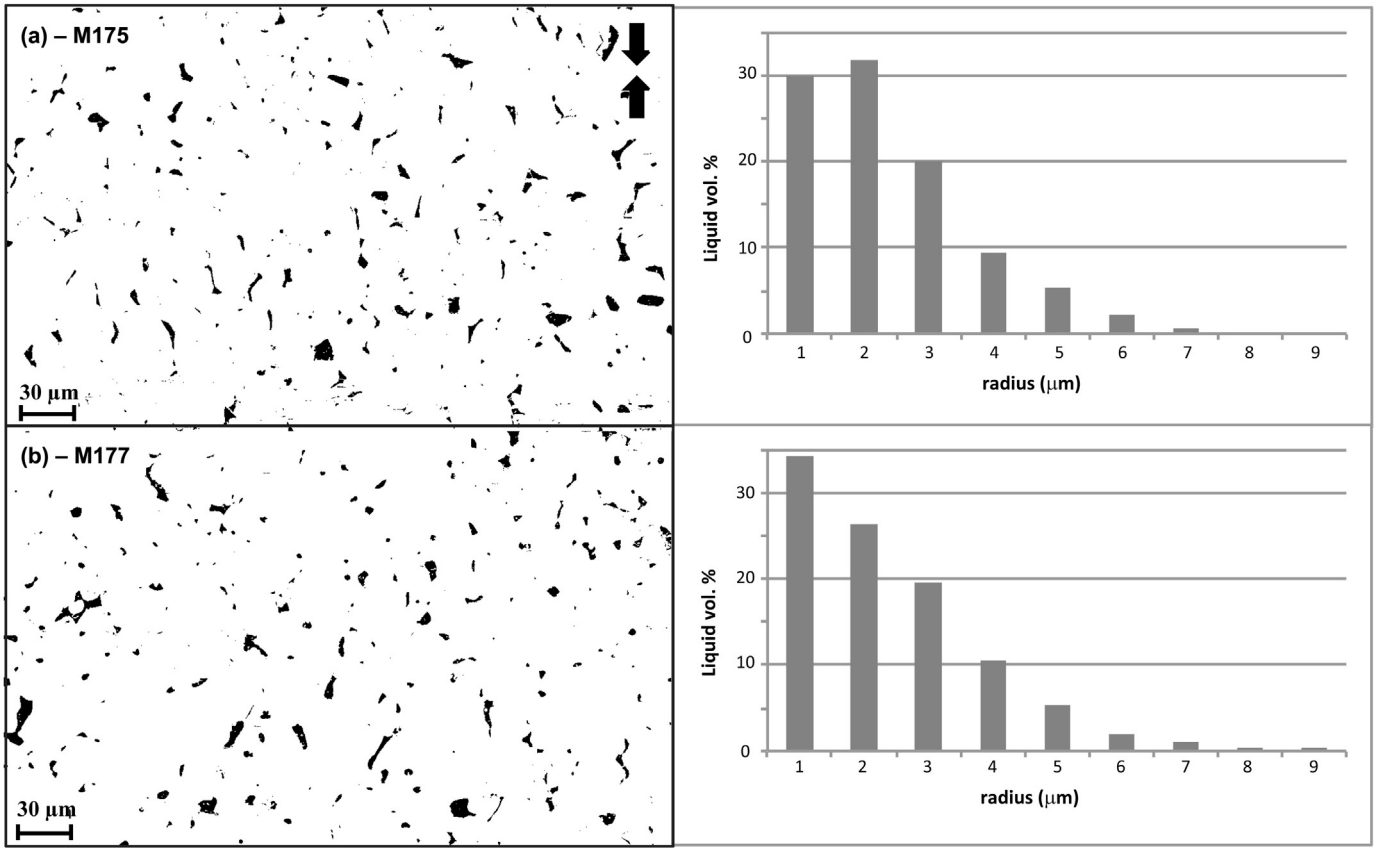


**Fig. 5.** Details of two silicate melt-free microstructures at a strain-rate of $1 \times 10^{-4}$ $s^{-1}$, after 15% shortening (a) and 35% finite shortening (b). Binary images show the elongated and distorted FeS microstructure (black). The liquid-pocket size versus liquid-fraction plot shows a preference for small pockets compared to basaltic-melt present experiments of Fig. 3. Note that M177 initially contained silicate melt that was expelled from the capsule during deformation. Black arrows indicate the shortening direction.

quench, respectively (Table 1). This decrease indicates some limited liquid segregation due to deformation.

Fig. 6 shows a direct comparison of the effect of basaltic melt on the deformation microstructure for two experimental runs that were deformed under the same conditions. The presence of basaltic melt causes (i) the FeS liquid pockets to be generally larger, and (ii) more equidimensional, and hence more isolated within the olivine crystals (see Fig. 3b and Fig. 5a for the liquid dis-

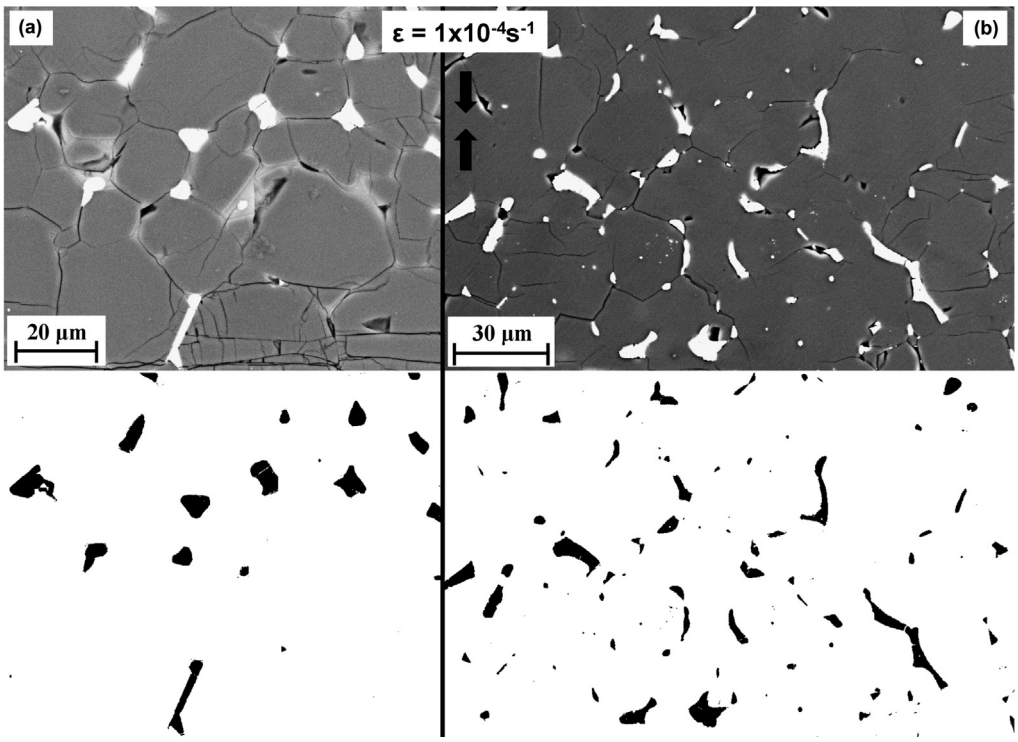


**Fig. 6.** BSE (top) and binary images (bottom), showing the effect of basaltic melt on the microstructures of two samples deformed under identical conditions. (a) M157, containing silicate melt, (b) M175, silicate melt-free. The addition of basaltic melt leads to larger and less elongated liquid pockets. Note that the lowermost liquid-pocket in (a) contains little or no basaltic melt, which explains its elongation similar to that observed in (b). Vertical arrows indicate the shortening direction.

tribution of these experiments). This demonstrates that the basaltic melt preferentially accommodates the strain under the experimental conditions, leaving the sulphide liquid pockets less disturbed. This generally hinders sulphide liquid interconnection and segregation compared to the silicate-melt free samples as evidenced by the reduced FeS liquid fraction observed after melt-free deformation.

## 4. Discussion

Several experimental studies have investigated the effect of basaltic melt on sulphide liquid interconnection and segregation from a peridotite or olivine matrix (Holzheid et al., 2000; Holzheid, 2013; Yoshino et al., 2004; Rushmer et al., 2005; Rushmer and Petford, 2011). To our knowledge, only Rushmer et al. (2005) performed deformation experiments in the two-liquid field using partially molten chondritic meteorite material. Unlike our experiments their samples displayed a much larger silicate melt fraction so that the two studies are not directly comparable. The study of Rushmer et al. (2005) mainly applies to liquid mobilization driven by impact events (e.g. Tomkins et al., 2013) after a large amount of silicate liquid has been formed, while our results can also be interpreted with respect to heating and thermal convection during planetary differentiation at a low degree of melting.

We have chosen a simplified system of olivine, basaltic melt and iron-sulphide liquid for our experiments. The biggest potential deviation from natural systems is the liquid composition that can strongly influence the dihedral angle (e.g. Terasaki et al., 2005). In progressively melting planetesimals the composition of Fe–Ni–S liquids evolves from sulphur-rich to Fe–Ni-rich, which leads to an increase of the dihedral angle and thereby reduces the potential for liquid interconnection and mobility with time. Thus, the choice of FeS as the Fe–Ni–S liquid phase analogue represents an upper bracket for liquid mobility in natural systems. In the following sections the effect of the basaltic melt on Fe–S liquid interconnection, distribution and segregation is discussed and the results are applied to the timing of planetary differentiation.

### 4.1. The effect of basaltic melt on Fe–S interconnection and segregation

Previous experimental studies have indicated that Fe–S liquid interconnection is significantly reduced by the addition of basaltic melt (e.g. Rushmer and Petford, 2011), and that silicate melting under static conditions only promotes Fe–S segregation at very high melt fractions (Holzheid et al., 2000; Holzheid, 2013). The reduced Fe–S interconnection in static systems can be explained by the interplay of two immiscible liquids with different surface energies. In such a system, the lower surface energy liquid is preferentially drawn into the narrow, high curvature grain intersections where even a small amount will isolate the higher surface energy liquid. At high temperatures the resulting pinch-off and rounding of Fe–S liquid-pockets occurs rapidly as reported by Yoshino et al. (2004), because the liquid–melt rearrangement does not require diffusive mass transport. This is in contrast to the slow pinch-off of metastable olivine–Fe–S liquid networks that require a sluggish liquid–grain rearrangement (Walte et al., 2007). This accelerated liquid–melt rearrangement process coupled with faster diffusive mass transfer through the silicate melt network explains the short annealing time that is required to achieve locally equilibrated FeS liquid pockets compared to silicate melt free experiments (ca. 1 h in this study compared to >14 h in Walte et al., 2007 for the olivine–FeS system).

Under the non-hydrostatic conditions considered in this study the local deformation in and around liquid pockets is an additional factor. In order to enhance liquid interconnection, e.g. by liquid pocket elongation in aggregates with a single liquid phase (e.g. olivine–FeS liquid), the differential stress $\Delta\sigma$ needs to exceed the shape-conserving capillary forces at the local melt-crystal boundaries. These can be expressed as the quotient of solid–liquid

surface energy $\gamma_{s-l}$ and the mean radius of curvature $r_{mean}$ (e.g. Kohlstedt and Holzman, 2009), leading to

$$k < \frac{\Delta\sigma \cdot r_{mean}}{\gamma_{s-l}} \tag{2}$$

with a constant $k = 1$ according to Groebner and Kohlstedt (2006) citing D. Stevenson (pers. comm.). If (2) is fulfilled, the system is dominated by deformation and therefore has the potential for increased interconnectivity; otherwise, the system is surface tension dominated and the liquid distribution is little effected regardless of the finite strain. Previous olivine–FeS deformation studies confirmed this interplay of surface tension with stress and showed that interconnection and liquid segregation can be enhanced if the strain rate is sufficiently high (Groebner and Kohlstedt, 2006; Walte et al., 2011). However, Walte et al. (2011) argued that the stress–surface tension dominated boundary was not sharp as assumed in (2), and that $k$ appeared to be significantly larger than unity based on a surface tension dominated regime that is larger than expected.

In a system with two melt phases the complex interplay of the two liquids with different solid–liquid surface energies and the sensitivity of the system to the volume fractions of the two liquids preclude the direct application of Eq. (2) to determine the liquid's response to deformation. For example, if the silicate melt fraction is significantly higher than the Fe–S liquid fraction, most of the Fe–S liquid would be surrounded by silicate melt and would therefore be shielded from the differential stress imposed on the grain framework and the silicate melt. Thus, the approach taken in this study was to investigate the threshold between surface tension dominated and stress dominated behavior empirically, while keeping the initial ratio of the two liquids constant. The quenched microstructures of a given deformation experiment can be visibly classified as dominated mainly by stress or by surface tension, when the overall liquid distribution is either distorted by deformation, or little effected, respectively (cf. Fig. 3). Since the stress needed to deform high dihedral angle liquid pockets is inversely proportional to the radius of curvature (Eq. (2)), individual liquid pockets from an experiment with a given differential stress, can be elongated and thus stress dominated or roundish and therefore surface tension dominated when they are larger and smaller, respectively. Thus, a graph of strain rate $\dot{\varepsilon}$ vs. liquid pocket radius of curvature $r$ can be plotted for the different experiments (Fig. 7). The experimental results are extrapolated to inaccessible low strain rates and larger liquid pocket sizes with the proportionality relation

$$r \propto \dot{\varepsilon}^{-1/n} \tag{3}$$

that can be derived from (2). A stress exponent for dislocation creep $n = 3.5$ is assumed in accordance with the olivine–FeS liquid experiments of Walte et al. (2011). Fig. 7 shows that the addition of basaltic melt enlarges the surface tension dominated field at the expense of the stress dominated field compared to basalt free experiments. Note that the exact boundary position is system specific and would likely change e.g. with a different basaltic melt–FeS liquid ratio. The extrapolation to natural Fe–S pocket sizes in the mm range shows that slow strain rates driven by thermal convection in larger (proto-) planets are unlikely to enhance liquid pocket interconnectivity. On the other hand, brief, high-strain rate events caused by impacts, can push the system into the stress dominated regime. We argue, however, that the interconnection is transient and will pinch-off immediately after the impact episode by the fast liquid–melt rearrangement described above.

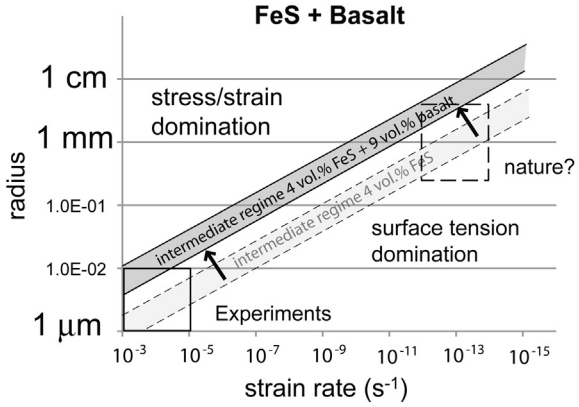


**Fig. 7.** Deformation regimes in a strain rate – liquid pocket size plot adapted from Walte et al. (2011). The addition of basaltic melt enlarges the field in which the FeS liquid pockets are surface tension dominated, i.e. liquid interconnection and therefore deformation aided percolation can only occur at higher strain rates that are likely not achievable during thermal convection in planetary bodies. The exact position of the boundary is determined by the liquid/melt fraction (see Section 4.1).

### 4.2. Liquid phase separation and the timing of planetary differentiation

Despite the evidence for liquid pinch-off after addition of silicate melt discussed above, early differentiation of planetesimals is often considered to happen contemporaneously by porous flow of Fe–Ni–S liquid to form a core and percolation of basaltic melt to form a proto-crust (e.g. Neumann et al., 2014). In fact, percolation of the core-forming melts above a certain volume threshold is often considered more efficient than basaltic percolation due to the higher density contrast with respect to olivine and the significantly lower viscosities of the metallic/sulphidic liquids compared to basaltic melt ($10^{-2}$–$10^{-3}$ Pa s, Dobson et al., 2000). The rapid separation of mobile basaltic melt from stranded FeS liquid observed in our experiments indicates the opposite. The interconnected silicate melt network allows the basalt to easily migrate along the hydraulic head out of the sample during deformation, while the low viscosity of FeS liquid does not enhance flow since no percolation network exists until the basalt is fully segregated. Under these circumstances the FeS liquid can only move through the silicate melt network in the form of isolated droplets. In order to fit through the narrow silicate melt tubules the droplets have to change shape, which requires a distorting stress that overcomes the pressure increase in the liquid pocket $\Delta P$ given by

$$\Delta P = \frac{2\gamma_{SL}}{R_{min}} - \frac{2\gamma_{SL}}{R_0} \tag{4}$$

(Mungall and Su, 2005) with the liquid–solid or liquid–melt surface energy $\gamma_{SL}$, the radius of a sphere with the liquid pocket volume $R_0$, and the smallest radius $R_{min}$ in the distorted state, which equals half the melt-tubule diameter. Considering a liquid pocket with an initial diameter of 5 mm ($R_0 = 2.5 \times 10^{-3}$ m), a maximum tubule width of 1 mm ($R_{min} = 5 \times 10^{-4}$ m), and a typical $\gamma_{SL} = 0.6$ J/m$^2$, $\Delta P$ equals only about 2 kPa, but would be significantly higher for a low silicate melt fraction (the lower the melt fraction the narrower the melt tubules of the melt network). This force could be provided by non-hydrostatic stress, viscous drag on the liquid pockets by melt flow, or by gravitational acceleration. Deformation and viscous drag by the outflowing melt were not sufficient to mobilize the liquid pockets in our experiments and according to the scaling considerations discussed in the previous section this would likely also not be the case under natural conditions. For planetesimal differentiation gravitational settling of FeS liquid may be the most interesting mechanism to consider, in this case the liquid pocket distorting stress would be provided by the gravitational force that acts on a given liquid pocket divided by the

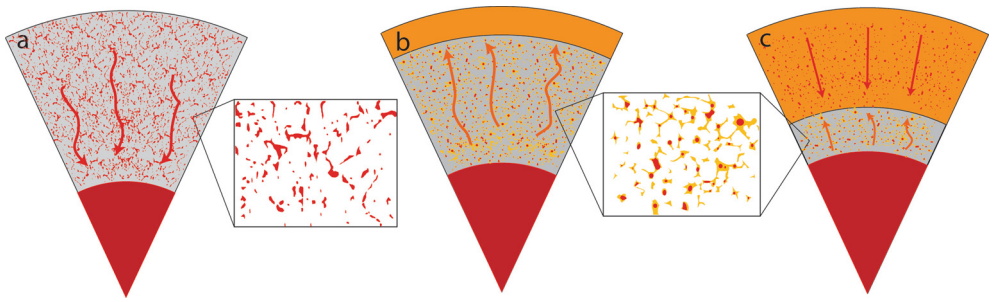


**Fig. 8.** Illustration of the inferred differentiation sequence for planetesimals. (a) Radiogenic heating causes the Fe–Ni–S solidus to be crossed; liquid percolates through a grain network to form the proto-core until a threshold of 5–10 vol.% residual liquid fraction is reached or until the silicate solidus is crossed (b). First basaltic melt immobilizes the remaining Fe–Ni–S liquid, but can percolate upwards to form a shallow melt layer. (c) A magma ocean stage and final Fe–Ni–S mobilization is only possible if radiogenic heating is sufficient.

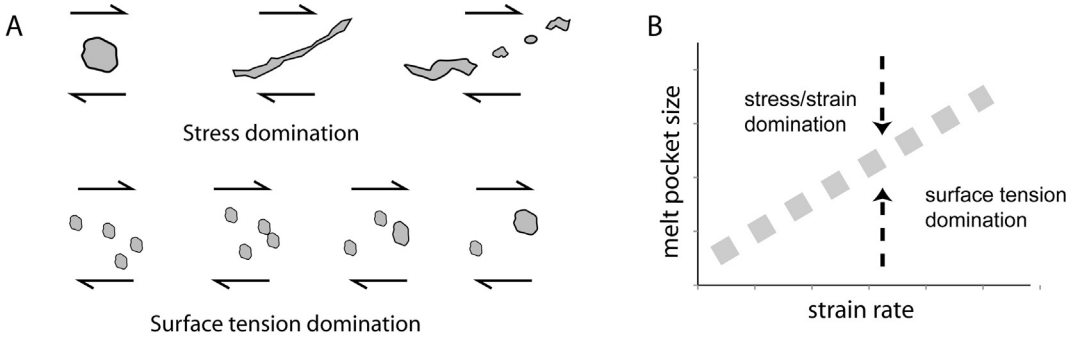


**Fig. 9.** Liquid pocket size evolution. (a) Schematic illustration of liquid pocket splitting and merging mechanisms. In the stress dominated regime liquid pockets are elongated, surface tension leads to a split and pinch-off into smaller, less elongated pockets. In the surface tension dominated regime (bottom) liquid pockets are little elongated but passively dragged within the matrix and coalesce into larger pockets. (b, redrawn from Walte et al., 2011) These mechanisms lead to an evolution of high dihedral angle systems towards the intermediate regime between stress and surface tension domination with progressive deformation.

silicate melt network tubule diameter through which the pocket should be squeezed: $\Delta P = \Delta\rho * V_{pocket} * g/(\pi R^2_{min})$. Using a solid–liquid density difference $\Delta\rho = 3 \times 10^{-3}$ kg/cm$^3$, $g = 0.2$ m/s$^2$ for a large planetesimal and the liquid pocket volume $V_{pocket}$ and melt tubule diameter $R_{min}$ of the example above results in a $\Delta P$ of only 50 Pa, which is nearly two orders of magnitude too low to overcome the surface tension of the liquid pocket so that liquid migration is inhibited (note that the liquid pocket deformation is not a process determined by viscosity but by surface tension, if the force is too small the pocket will not move even in geological time-scales). The liquid pocket settling at 15 vol.% of silicate melt reported by Bagdassarov et al. (2009b) can be explained by the enhanced gravitational acceleration in their centrifuge experiments.

Thus, under low-g conditions of planetesimal differentiation Fe–Ni–S liquids are immobile after the silicate solidus is overstepped as long as upward silicate melt migration balances new melt formation to keep the melt fraction low. Fig. 8 summarizes the consequences for the timing of differentiation of planetesimals such as 4 Vesta. The most important point is that core–mantle differentiation in planetesimals that have not experienced a major magma ocean stage is likely confined to a narrow "window of opportunity" temperature interval of as little as 50 K above the Fe–Ni–S solidus and below the silicate solidus. Hence, the sulfur content is vital for the early differentiation, since a higher sulfur ratio raises the amount of liquid that is formed in that temperature interval and lowers the dihedral angle, which increases connectivity and percolation. This is confirmed by the correlation between sulfur content and formation age of iron meteorites reported by Kruijer et al. (2014).

### 4.3. Liquid accumulation vs. liquid dispersion

Besides tracking changes in the FeS liquid fraction in the recovered samples and observing the distortion of liquid pockets as an indication for liquid interconnection and segregation, investigating the evolution of the liquid distribution within the sample provides additional information for potential segregation and accumulation processes. A liquid with a dihedral angle above 60° can only form an interconnected network close to the interconnection melt fraction (cf. Von Bargen and Waff, 1986) when the liquid is evenly dispersed within the matrix. The localized concentration of liquid pockets would reduce the tendency for the liquid to interconnect (Walte et al., 2007). On the other hand, accumulation of liquid in progressively growing pockets may be the beginning of stepwise accumulation and large-scale non-continuous liquid migration as considered by Bons et al. (2004) for example. In order to understand whether the increasing liquid-pocket sizes observed in all two-liquid experiments (except at the fastest strain rates) initiate a run-away accumulation process, the underlying liquid accumulation and dispersion processes have to be considered. In general, liquid accumulation is energetically favorable in solid–liquid systems with a dihedral angle larger than ~70° (note that this threshold is larger than the full interconnectivity angle of 60°, see Jurewicz and Watson, 1985). This tendency of the isolated liquid pockets to grow relies on slow diffusive processes (Ostwald ripening) or on coalescence when they come into contact with each other during grain growth or deformation. In deforming environments liquid pocket growth may be counteracted by dispersion processes that preferentially act on larger liquid pockets (Fig. 9a). Hence, liquid pocket growth is observed in static environments or during deformation in the surface tension dominated regime, liquid pocket splitting and dispersion is observed in the stress dominated regime (Walte et al., 2011). At a given

steady state strain rate the average liquid pocket size can therefore be expected to evolve towards the intermediate deformation regime (Fig. 9b), which explains the liquid pocket size increase observed in our moderate and low strain rate experiments (surface tension dominated) and the liquid pocket size decrease in the FeS–olivine deformation experiments of Walte et al. (2011) that were conducted in the stress dominated regime. For example, in a hypothetical proto-planet with slow internal convection, regardless of initial liquid pocket size distribution, the Fe–S liquid pocket size would evolve into the cm range as long as both Fe–S liquid and silicate melt were present according to Fig. 7. However, after the basaltic melt has been segregated the deforming system would find itself in the stress dominated regime and the liquid pocket size would evolve towards the mm range by splitting and dispersion, which could enhance liquid segregation as observed in our high finite strain experiments. Thus, the liquid pocket size increase observed in our experiments is likely self-limited and does not initiate liquid accumulation above the mm to cm range that could lead to large-scale differentiation unless additional mechanisms such as diking contribute to further accumulation.

## 5. Conclusions

In order to investigate the potential for deformation-assisted core–mantle differentiation in the early history of planetesimals, we performed a systematic study deforming a polycrystalline olivine aggregate that contains a low fraction of two immiscible liquids with high and low dihedral angles, respectively. It was found that the addition of a low percentage of basaltic melt to a system containing metallic or sulphidic liquid does not aid segregation of the latter but rather inhibits any previously established sulphidic liquid network that could have led to partial (but incomplete) core–mantle differentiation. Additionally, it was shown that the deforming system containing two immiscible liquid phases is unstable and transient. Even after a moderate finite strain the silicate melt phase is efficiently segregated leaving the sulphide liquid droplets stranded in the matrix. If core–mantle differentiation requires an early episode of porous Fe–S segregation as recent investigations of iron meteorites seem to indicate (Kruijer et al., 2014), it must have occurred before the silicate solidus was overstepped and was likely aided by episodes of deformation to avoid a pinch-off of the liquid network.

## Acknowledgements

We thank two anonymous reviewers for thoughtful comments that helped to improve and clarify the manuscript. N.P.W. was supported by the Federal Ministry of Education and Research (BMBF) project 05K13WC1. D.C.R. was supported by the European Research Council (ERC) Advanced Grant “ACCRETE” (contract number 290568).

## Appendix A. Supplementary material

Supplementary material related to this article can be found online at http://dx.doi.org/10.1016/j.epsl.2015.02.014.

## References

Bagdassarov, N., Golabek, G.J., Solferino, G., Schmidt, M.W., 2009a. Constraints on the Fe–S melt connectivity in mantle silicates from electrical impedance measurements. Phys. Earth Planet. Inter. 177, 139–146.

Bagdassarov, N., Solferino, G., Golabek, G.J., Schmidt, M.W., 2009b. Centrifuge assisted percolation of Fe–S melts in partially molten peridotite: time constraints for planetary core formation. Earth Planet. Sci. Lett. 288, 84–95.

Ballhaus, C., Ellis, D.J., 1996. Mobility of core melts during Earth's accretion. Earth Planet. Sci. Lett. 143, 137–145.

Bons, P.D., Arnold, J., Elburg, M.A., Kalda, J., Soesoo, A., van Milligen, B.P., 2004. Melt extraction and accumulation from partially molten rocks. Lithos 78, 25–42.

Bruhn, D., Groebner, N., Kohlstedt, D.L., 2000. An interconnected network of core-forming melts produced by shear deformation. Nature 403, 883–886.

Bulau, J.R., Waff, H.S., Tyburczy, J.A., 1979. Mechanical and thermodynamic constraints on fluid distribution in partial melts. J. Geophys. Res. 84, 6102–6108.

Dobson, D.P., Crichton, W.A., Vocadlo, L., Jones, A.P., Wang, Y., Uchida, T., Rivers, M., Sutton, S., Brodholt, J.P., 2000. In situ measurement of viscosity of liquid in the Fe–FeS system at high pressures and temperatures. Am. Mineral. 85, 1838–1842.

Groebner, N., Kohlstedt, D.L., 2006. Deformation-induced metal melt networks in silicates: implication for core–mantle interactions in planetary bodies. Earth Planet. Sci. Lett. 245, 571–580.

Gupta, G., Sahijpal, S., 2010. Differentiation of Vesta and the parent bodies of other achondrites. J. Geophys. Res. 115. http://dx.doi.org/10.1029/2009JE003525.

Hevey, P.J., Sanders, I.S., 2006. A model for planetesimal meltdown by $^{26}$Al and its implications for meteorite parent bodies. Meteorit. Planet. Sci. 41, 95–106.

Holzheid, A., Schmitz, M.D., Grove, T.L., 2000. Textural equilibria of iron sulfide liquids in partly molten silicate aggregates and their relevance to core formation scenarios. J. Geophys. Res. 105, 555–567.

Holzheid, A., 2013. Sulphide melt distribution in partially molten silicate aggregates: implications to core formation scenarios in terrestrial planets. Eur. J. Mineral. 25, 267–277.

Hustoft, J.W., Kohlstedt, D.L., 2006. Metal-silicate segregation in deforming dunitic rocks. Geochem. Geophys. Geosyst. 7, Q02001. http://dx.doi.org/10.1029/2005GC001048.

Jurewicz, S.R., Watson, E.B., 1985. The distribution of partial melt in a granitic system: the application of liquid phase sintering theory. Geochim. Cosmochim. Acta 49, 1109–1121.

Kinzler, R.J., Grove, T.L., 1992. Primary magmas of mid-ocean ridge basalts 2. Applications. J. Geophys. Res. 97, 6907–6926.

Kohlstedt, D.L., Holzman, B.K., 2009. Shearing melt out of the Earth. Annu. Rev. Earth Planet. Sci. 37, 561–593.

Kruijer, T.S., Touboul, M., Fischer-Gödde, M., Bermingham, K.R., Walker, R.J., Kleine, T., 2014. Protracted core formation and rapid accretion of protoplanets. Science 344, 1150–1154.

Manthilake, M.A.G.M., Walte, N., Frost, D.J., 2012. A new multi-anvil press employing six independently acting 8 MN hydraulic rams. High Press. Res. 32 (2). http://dx.doi.org/10.1080/08957959.2012.680450.

Mungall, J.E., Su, S., 2005. Interfacial tension between magmatic sulfide and silicate liquids: constrains on kinetics of sulfide liquation and sulfide migration through silicate rocks. Earth Planet. Sci. Lett. 234, 135–149.

Neumann, W., Breuer, D., Spohn, T., 2014. Differentiation of Vesta: implications for a shallow magma ocean. Earth Planet. Sci. Lett. 395, 267–280.

Rose, L.A., Brenan, J.M., 2001. Wetting properties of Fe–Ni–Co–Cu–O–S melts against olivine: implications for sulfide meltmobility. Econ. Geol. 96, 145–157.

Rosenberg, C.L., Handy, M.R., 2001. Mechanisms and orientation of melt segregation paths during pure shearing of a partially molten rock analog (norcamphor–benzamide). J. Struct. Geol. 23, 1917–1932.

Rubie, D.C., Melosh, H.J., Reid, J.E., Liebske, C., Righter, K., 2003. Mechanisms of metal-silicate equilibration in the terrestrial magma ocean. Earth Planet. Sci. Lett. 205, 239–255.

Rubie, D.C., Nimmo, F., Melosh, H.J., 2007. Formation of Earth's core. Treatise Geophys. 9, 51–90.

Rushmer, T., Petford, N., 2011. Microsegregation rates of liquid Fe–Ni–S metal in natural silicate-metal systems: a combined experimental and numerical study. Geochem. Geophys. Geosyst. 12. http://dx.doi.org/10.1029/2010GC003413.

Rushmer, T., Petford, N., Humayun, M., Campbell, A.J., 2005. Fe-liquid segregation in deforming planetesimals: coupling core-forming compositions with transport phenomena. Earth Planet. Sci. Lett. 239, 185–202.

Stevenson, D.J., 1990. Fluid dynamics of core formation. In: Newsom, H.E., Jones, J.H. (Eds.), Origin of the Earth. Oxford University Press, New York, pp. 29–43.

Terasaki, H., Frost, D.J., Rubie, D.C., Langenhorst, F., 2005. The effect of oxygen and sulphur on the dihedral angle between Fe–O–S melt and silicate minerals at high pressure: implications for Martian core formation. Earth Planet. Sci. Lett. 232, 379–392.

Terasaki, H., Frost, D.J., Rubie, D.C., Langenhorst, F., 2008. Percolative core formation in planetesimals. Earth Planet. Sci. Lett. 273, 132–137.

Tomkins, A.G., Weinberg, R.F., Schaefer, B.F., Langendam, A., 2013. Disequilibrium melting and melt migration driven by impacts: implications for rapid planetesimal core formation. Geochim. Cosmochim. Acta 100, 41–59.

Von Bargen, N., Waff, H.S., 1986. Permeabilities, interfacial areas and curvatures of partially molten systems: results of numerical computation of equilibrium microstructures. J. Geophys. Res. 91, 9261–9276.

Wang, Y., Durham, W.B., Getting, I.C., Weidner, D.J., 2003. The deformation-DIA: a new apparatus for high temperature triaxial deformation to pressures up to 15 GPa. Rev. Sci. Instrum. 74, 3002–3011.

Walte, N.P., Becker, J.K., Bons, P.D., Rubie, D.C., Frost, D.J., 2007. Liquid distribution and attainment of textural equilibrium in a partially-molten crystalline system with a high-dihedral-angle liquid phase. Earth Planet. Sci. Lett. 262, 517–532.

Walte, N.P., Bons, P.D., Passchier, C.W., Koehn, D., 2003. Disequilibrium melt distri-

bution during static recrystallization. Geology 31, 1009–1012.
Walte, N.P., Rubie, D.C., Bons, P.D., Frost, D.J., 2011. Deformation of a crystalline aggregate with a small percentage of high-dihedral-angle liquid: implications for core–mantle differentiation during planetary formation. Earth Planet. Sci. Lett. 305, 124–134.
Walter, M.J., Trønnes, R.G., 2004. Early Earth Differentiation. Earth Planet. Sci. Lett. 225, 253–269.
Wilson, L., Keil, K., 2012. Volcanic activity on differentiated asteroids: a review and analysis. Chem. Erde 72, 289–321.
Wood, B.J., Walter, M.J., Wade, J., 2006. Accretion of the Earth and segregation of its core. Nature 44, 825–833.
Yoshino, T., Walter, M.J., Katsura, T., 2003. Core formation in planetesimals triggered by permeable flow. Nature 422, 154–157.
Yoshino, T., Walter, M.J., Katsura, T., 2004. Connectivity of molten Fe alloy in peridotite based on in situ electrical conductivity measurements: implications for core formation in terrestrial planets. Earth Planet. Sci. Lett. 222, 625–643.